

Environmental and vegetational changes recorded in sedimentary leaf wax n-alkanes across the Cretaceous-Paleogene boundary at Loma Capiro, Central Cuba

メタデータ	言語: English 出版者: 公開日: 2017-10-03 キーワード: 作成者: Yamamoto, Shinya, Hasegawa, Takashi, Tada, Ryuji, Goto, Kazuhisa, Reinaldo, Rojas-Consuegra, Diaz-Otero, Consuelo, Garcia-Delgado, Dora E., Yamamoto, Shinji, Sakuma, Hironobu, Matsui, Takafumi, 長谷川, 卓 メールアドレス: 所属:
URL	https://doi.org/10.24517/00010957

This work is licensed under a Creative Commons Attribution-NonCommercial-ShareAlike 3.0 International License.



1 Environmental and vegetational changes recorded in sedimentary leaf wax *n*-alkanes
2 across the Cretaceous–Paleogene boundary at Loma Capiro, Central Cuba

3
4 Shinya Yamamoto^{a,*}, Takashi Hasegawa^a, Ryuji Tada^b, Kazuhisa Goto^{c,1}, Reinaldo
5 Rojas-Consuegra^d, Consuelo Díaz-Otero^e, Dora E. García-Delgado^f, Shinji Yamamoto^b,
6 Hironobu Sakuma^b, Takafumi Matsui^{g,1}

7
8 ^a*Department of Earth Sciences, Graduate School of Natural Science and Technology,*
9 *Kanazawa University, Kakuma, Kanazawa 920-1192, Japan*

10 ^b*Department of Earth and Planetary Science, Graduate School of Science, The*
11 *University of Tokyo, 7-3-1 Hongo, Tokyo 113-0033, Japan*

12 ^c*Disaster Control Research Center, Graduate School of Engineering, Tohoku University,*
13 *Aoba 06-6-11, Aramaki, Sendai 980-8579, Japan*

14 ^d*Museo Nacional de Historia Natural, Obispo No. 61, Plaza de Armas, La Habana*
15 *Vieja 10100, Cuba*

16 ^e*Instituto de Geología y Paleontología Vía Blanca y Línea del Ferrocarril. San Miguel*
17 *del Padrón, La Habana 11 000, Cuba*

18 ^f*Centro de Investigaciones del Petróleo, Washington No. 166, esquina Churruca,*
19 *Municipio Cerro, Ciudad de la Habana, Cuba*

20 ^g*Department of Complexity Science and Engineering, Graduate School of Frontier*
21 *Science, The University of Tokyo, 7-3-1 Hongo, Tokyo 113-0033, Japan*

22
23 * Corresponding author. Present address: Institute of Low Temperature Science,
24 Hokkaido University, N19W8, Kita-ku, Sapporo 060-0819, Japan. Fax:
25 +81-11-706-7142.

26 *E-mail address:* s.yamamoto@pop.lowtem.hokudai.ac.jp (S. Yamamoto)

27 ¹ Present address: Planetary Exploration Research Center, Chiba Institute of Technology,
28 2-17-1 Tsudanuma, Narashino 275-0016, Chiba, Japan.

29

30 ABSTRACT

31 The stable carbon isotopic compositions ($\delta^{13}\text{C}$) and chain-length distribution [ACL and
32 $n\text{-C}_{31}/(n\text{-C}_{29}+n\text{-C}_{31})$] of sedimentary leaf wax *n*-alkanes were investigated across the
33 Cretaceous–Paleogene (K–Pg) boundary at Loma Capiro, Central Cuba, to reconstruct
34 paleoenvironmental changes that are recorded in terrestrial higher plants. The
35 stratigraphic profiles of the *n*-alkane $\delta^{13}\text{C}$ values show a negative excursion in the
36 lowermost Paleocene, although its magnitude is much smaller ($\sim 0.3\%$) than the global
37 signals (1.5 to 2.0‰) in the surface ocean-atmospheric carbon reservoir. Relations
38 between the *n*-alkane $\delta^{13}\text{C}$ values and the $\text{C}_{31}/(\text{C}_{29} + \text{C}_{31})$ ratios exhibit two different
39 trends, suggesting that our $\delta^{13}\text{C}$ records are likely affected by two types of
40 paleoenvironmental factors in addition to the $\delta^{13}\text{C}$ variations in the exogenous carbon
41 reservoir. Rare occurrence of terrigenous organic matter that is usually transported by
42 rivers suggests that the *n*-alkanes at Loma Capiro are likely to have been transported by
43 trade winds, which recorded paleoenvironmental conditions of the northwestern part of
44 the African continent. The *n*-alkane $\delta^{13}\text{C}$ values show a parallel decrease with the ACL
45 and $\text{C}_{31}/(\text{C}_{29} + \text{C}_{31})$ values in the first 37,000 yrs following the K–Pg boundary. Such
46 decreases are consistent with plant physiological responses to reduced net evaporation,
47 suggesting a possible influence of the impact-induced warm-humid condition in the
48 early Paleocene. In contrast, the *n*-alkane $\delta^{13}\text{C}$ values are negatively correlated with the
49 $\text{C}_{31}/(\text{C}_{29} + \text{C}_{31})$ ratios from 40,000 to 67,000 yrs after the K–Pg boundary. This time
50 period matches well with that required for the recovery of terrestrial floras from the
51 K–Pg mass extinction to those with diversity equivalent to the late Cretaceous,
52 suggesting that the *n*-alkane signals are also likely affected by the plant diversification

53 process after the mass extinction.

54

55 *Keywords:* K–Pg boundary, Cretaceous, Paleogene, stable carbon isotopes, *n*-alkane,

56 leaf wax

57 **1. Introduction**

58 The mass extinction event at the Cretaceous–Paleogene (K–Pg) boundary is
59 one of the five largest mass extinction events in the Phanerozoic. More than 15% of
60 fossil families went extinct in the ocean (Raup and Sepkoski, 1982), and 15% to 57% of
61 diverse Cretaceous flora abruptly disappeared on land (Orth et al., 1981; Wolfe and
62 Upchurch, 1987; Johnson et al., 1989; Vajda and Raine, 2003; Wilf and Johnson, 2004;
63 Nichols, 2007). The stable carbon isotopic compositions ($\delta^{13}\text{C}$) of the surface ocean (e.g.
64 Hsü et al., 1982; Gilmour et al., 1987; Keller and Lindinger, 1989; Meyers and Simoneit,
65 1990; Meyers, 1992; Hollander et al., 1993) and terrestrial sedimentary carbon
66 (Schimmelmann and DeNiro, 1984; Arinobu et al., 1999; Arens and Jahren, 2000, 2002)
67 show an abrupt negative excursion at the K–Pg boundary, suggesting a large impact of
68 this mass extinction on global carbon cycles. Combined stratigraphical,
69 micropaleontological, petrological and geochemical data show that this mass extinction
70 was triggered by a large asteroid impact at Chicxulub on Yucatan peninsula, Mexico
71 (Schulte et al., 2010).

72 The $\delta^{13}\text{C}$ values of terrestrial higher plants are primarily controlled by the
73 isotopic composition of atmospheric CO_2 (Farquhar et al., 1982; Arens et al., 2000).
74 Therefore, stratigraphic records of plant $\delta^{13}\text{C}$ values can provide good constraints on the
75 rate and magnitude of disruption in the global carbon cycles. The $\delta^{13}\text{C}$ excursion in
76 sedimentary leaf wax *n*-alkanes implies a loss of at most 24% of the Cretaceous
77 biomass at the boundary (Arinobu et al., 1999).

78 On the other hand, the $\delta^{13}\text{C}$ values of terrestrial higher plants are also
79 sensitive to isotopic fractionations that reflect ecological and physiological responses to
80 their growing environment (Farquhar et al., 1989; Arens et al., 2000), as well as
81 taxonomic variations within contributing plant communities (Arens and Jahren, 2002).
82 Because abundant evidences suggest a global turnover in vegetation (Vajda and Raine,
83 2003) and changes in continental climate (Wolfe and Upchurch, 1987; Wolfe, 1990;
84 Lehman, 1990) at the K–Pg boundary, these changes might have affected the $\delta^{13}\text{C}$
85 values of terrestrial higher plants. In fact, the magnitudes of the $\delta^{13}\text{C}$ excursions
86 recorded in terrigenous organic matter across the K–Pg boundary range from -1.1 to
87 -2.8‰ (Arinobu et al., 1999; Arens and Jahren, 2000, 2002), exhibiting much larger
88 variations than those caused by the plant vital effects ($\sim 0.8\text{‰}$; Arens and Jahren, 2002).
89 However, the causes for these $\delta^{13}\text{C}$ variations still remain unclear.

90 Several studies have shown that comparison of the $\delta^{13}\text{C}$ fluctuations of
91 terrigenous organic matter with those in the exogenous carbon reservoir, such as marine
92 carbonate, is useful to reconstruct paleoenvironmental signals that are recorded in
93 terrestrial higher plants (e.g. Hasegawa et al., 2003). However, this approach cannot be
94 utilized for K–Pg boundary sequences because the shape and magnitude of the $\delta^{13}\text{C}$
95 changes of marine carbonates are also affected by changes in calcareous microfossil
96 compositions, size distributions of planktonic foraminiferal species, and local
97 productivity (D’Hondt and Zachos, 1993; Barrera and Keller, 1994).

98 Long chain (C_{27} to C_{33}) *n*-alkanes with an odd/even carbon number
99 predominance are typical of terrestrial higher plant waxes (Eglinton and Hamilton,
100 1967). These *n*-alkanes are ubiquitous in marine sediments (Pancost and Boot, 2004),
101 and their chain-length distributions are sensitive to changes in the plant growing
102 environment and the composition of their source vegetation (Hall and Jones, 1961;
103 Poynter et al., 1989; Schefuß et al., 2003; Sachse et al., 2006). Hence, we assess

104 paleoenvironmental conditions that may have been recorded in terrestrial higher plants
105 using two *n*-alkane biomarker proxies based on their chain length distribution, i.e., the
106 average chain length (ACL₂₇₋₃₃) and the C₃₁/(C₂₉ + C₃₁) ratio. The ACL₂₇₋₃₃ is the
107 concentration-weighted mean chain length of the C₂₇ to C₃₃ odd carbon number
108 *n*-alkanes (Poynter et al., 1989), and its variations are generally related to environmental
109 changes such as the temperature and aridity in which their source vegetation grows
110 (Gagosian and Peltzer, 1986; Poynter et al., 1989; Schefuß et al., 2003;
111 Rommerskirchen et al., 2003). In contrast, the C₃₁/(C₂₉ + C₃₁) ratio is the concentration
112 ratio of the C₃₁ *n*-alkanes to the sum of the C₂₉ and C₃₁ *n*-alkanes (Schefuß et al., 2003),
113 and its variations are more closely related to changes in aridity, than in temperature and
114 vegetation type (Schefuß et al., 2003).

115 The ultimate objective of this study is to reconstruct the environmental and
116 vegetational changes that may be recorded in the δ¹³C variations across the K–Pg
117 boundary. Here we report the results from the hemipelagic K–Pg sequence at Loma
118 Capiro, central Cuba, in which a published planktonic foraminiferal biostratigraphy
119 (Alegret et al., 2005) and a high sedimentation rate allow us to conduct a
120 stratigraphically well-constrained, high-resolution analysis of this boundary sequence.

121 **2. Setting and stratigraphy of Loma Capiro**

122 Loma Capiro is a small hill of ca. 180 m height in the northeast part of the
123 Santa Clara city, central Cuba (Fig. 1), that provides an excellent exposure of the K–Pg
124 boundary sequence on its southern slope. The K–Pg boundary sequence at Loma Capiro
125 is composed of a hemipelagic sequence of foraminifera-rich massive gray calcareous
126 mudstone and sandstone, and a 10.9 m-thick clastic complex (Fig. 2). These sediments
127 are included in the upper Maastrichtian Santa Clara Formation and the Paleocene Ochoa
128 Formation (Rojas-Consuegra et al., 2007). Paleogeographic reconstructions suggest that

129 the K–Pg location of the site was about 500 km south of its present position and that its
130 sediment accumulated on the northeastern slope of the Cuban carbonate platform on the
131 south edge of the proto-Caribbean Basin (Fig. 1d; Rojas-Consuegra et al., 2005;
132 Núñez-Cambra and Rojas-Consuegra, 2007; Goto et al., 2008). Benthic foraminiferal
133 assemblages indicate a paleodepth of 700 m to 3,000 m (Alegret et al., 2005).

134 The lithology of uppermost 1.5 m of the Maastrichtian is marked by
135 well-lithified gray calcareous mudstone followed by a continuous upward-fining
136 sequence of the clastic complex with an erosional contact (Fig. 2). The basal 6.5 m of
137 the sequence is characterized by a matrix-supported breccia with siltstone to very fine
138 sandstone matrix and rounded clasts of mudstone, limestone, gabbro and serpentinite.
139 Diameters of these clasts are generally less than 10 cm. Neither imbrication nor changes
140 in grain size are observed. The subsequent 1.5 m of the sequence is upward-fining
141 microbreccia with cross lamination, which is overlain by 65 cm-thick medium to coarse
142 sandstones. The uppermost 2.5 m of the complex is composed of an upward-fining
143 sequence of coarse-medium to medium-fine sandstones with intercalations of 15
144 cm-thick limestone and 10 cm-thick whitish clay layers.

145 Similar end-Cretaceous clastic deposits have been widely recognized around
146 the Gulf of Mexico and in the proto-Caribbean Sea (Smit et al., 1996; Tada et al., 2003;
147 Schulte et al., 2006; Goto et al., 2008). Lithologic and paleontologic evidence suggests
148 that these sediments were deposited in a geologically instantaneous period by the
149 collapse of carbonate platforms, gravity flows and large tsunamis that are associated
150 with the K–Pg impact at Chicxulub (Bralower et al., 1998). Likewise, the presence of
151 reworked Cretaceous foraminifera and impact materials in the clastic complex at Loma
152 Capiro suggests its link to the K–Pg impact (Alegret et al., 2005). We therefore placed
153 the K–Pg boundary at the bottom of the clastic complex (= basal 0 in Fig. 2).

154 The boundary between the clastic complex and the Paleocene mudstone is

155 sharp and marked by light to dark gray mudstone that has a strike of N75°E and a
156 northward dip of 56° (Fig. 1c). The lower half of the Paleocene sequence is mainly
157 composed of light gray to brownish gray mudstone with intercalations of sandstone
158 layers. In contrast, the upper half of the sequence is generally characterized by
159 alternating beds of light gray to reddish brown mudstone and 1 to 15 cm-thick light gray
160 fine to medium sandstone. An intercalation of ca. 50 cm-thick fine to medium sandstone
161 is observed at the 454 cm horizon above the clastic complex (Fig. 2).

162 Three planktonic foraminiferal datums are assigned to the 200 cm, 248.7 cm
163 and 520 to 620 cm horizons above the clastic complex by comparison to the results of
164 Alegret et al. (2005) (Fig. 2). The ages of these datums are 64.9 Ma, 64.5 Ma and 63.0
165 Ma, respectively (Berggren et al., 1995). Linear sedimentation rates (LSR) of the
166 Paleocene sequence above the clastic complex are therefore calculated as 2.0 cm/kyr for
167 the 0–200 cm, 0.1 cm/kyr for the 200–248.7 cm, and 0.2 cm/kyr for the 248.7–620 cm
168 interval.

169 **3. Materials and Methods**

170 *3.1. Samples*

171 Samples were obtained from the upper 1.5 m of the Maastrichtian calcareous
172 mudstone and the lower 11 m of the Paleocene mudstone above the clastic complex (Fig.
173 2). We did not collect samples from the complex because it is mainly composed of
174 reworked Cretaceous materials that the impact left behind, and therefore we put a 0
175 horizon for the Paleocene sequence at the top of the clastic complex (= top 0 in Fig. 2).
176 We used two slightly separated transects for sampling because the vertical exposure that
177 contained the Maastrichtian section did not allow collection of stratigraphically
178 continuous Paleocene samples. Both transects are well correlated by the upper boundary

179 of the clastic complex. The outcrop was trenched to about 1 m to obtain fresh
180 unweathered samples. Sampling resolutions that are estimated from the LSRs of the
181 Paleocene range from several thousand years to several hundreds of thousand years.

182 3.2. Measurements of calcium carbonate (CaCO_3) and total organic carbon (TOC) 183 concentrations

184 Powdered samples were treated with 5N-HCl for 24h to remove carbonate
185 minerals. Subsequently, the sediments were rinsed with deionized water to remove
186 CaCl_2 and dried in an oven (60 °C). The concentrations of calcium carbonate were
187 calculated using weight differences before and after the acid treatment. Measurements
188 of total organic carbon (TOC) content were performed on a Thermo Finnigan FlashEA
189 1112 elemental analyzer at the Center for Marine Core Research, Kochi University.

190 3.3. Organic geochemical analysis

191 3.3.1. Extraction and separation

192 The samples were powdered in an agate mill after removal of surface
193 contaminants and drying in an oven (60 °C) overnight. Finely ground samples (ca. 25–
194 120 g) were Soxhlet extracted with CH_2Cl_2 (DCM) for 48 h. The extracts were
195 separated into aliphatic, aromatic, ketone and polar fractions using silica gel column
196 chromatography (5% H_2O deactivated) by elution with *n*-hexane (2 ml), *n*-hexane/DCM
197 (3:1, v/v, 3 ml), DCM (3 ml) and DCM/MeOH (4:1, v/v, 4 ml), respectively. Blank tests
198 showed that there was no laboratory contamination of *n*-alkanes during the procedure.
199 These lipid fractions were analyzed using gas chromatography (GC) and GC/mass
200 spectrometry (MS) at Kanazawa University. For compound-specific stable carbon
201 isotope analyses, sufficient amounts of *n*-alkanes were purified using the urea adduction
202 technique (Hasegawa et al., 2006) and then determined by GC/isotope ratio monitoring

203 MS (GC/irmMS) at the Center for Marine Core Research, Kochi University.

204 3.3.2. GC and GC/MS

205 GC analysis was performed using a Hewlett-Packard 6890 gas chromatograph
206 equipped with an on-column injector, an HP-1 fused silica capillary column (30 m ×
207 0.32 mm i.d., 0.25 μm film thickness) connected with 5 m guard column and a flame
208 ionization detector (FID). Helium was used as the carrier gas. The GC oven temperature
209 was programmed from 50 °C to 120 °C at 30 °C/min, then to 310 °C at 5 °C/min and
210 held isothermally for 19.57 min. GC/MS analysis was performed using a
211 Hewlett-Packard 5973 Mass Selective Detector coupled to a Hewlett-Packard 6890 GC
212 equipped with a HP-5MS fused silica capillary column (30 m × 0.25 mm i.d., 0.25 μm
213 film thickness) and split/splitless injector. The temperature program was the same as for
214 GC analysis. The MS was operated in Electron-Impact mode at 70 eV, scanning a mass
215 range of m/z 40-650 at 2.44 scans per second. The compounds were identified on the
216 basis of their mass spectra, GC retention times, and comparison with literature spectra.

217 3.3.3. Compound-specific carbon isotope analysis

218 $^{13}\text{C}/^{12}\text{C}$ ratios of individual n -alkanes were determined using a Finnigan MAT
219 Delta ^{plus} XP mass spectrometer interfaced with a Trace GC, via a combustion furnace
220 maintained at 840 °C. The GC was equipped with a HP-5MS fused silica capillary
221 column (30 m × 0.32 mm i.d., 0.25 μm film thickness) and split/splitless injector.
222 Helium was used as the carrier gas. The GC oven was ramped from 50 °C to 310 °C at
223 4 °C/min and held isothermally for 25 min. CO₂ gas with a pre-calibrated isotopic
224 composition was used as a standard. The $\delta^{13}\text{C}$ values are expressed as per mil (‰)
225 relative to the Vienna Pee Dee Belemnite (VPDB). A standard mixture consisting of C₁₆
226 to C₃₀ n -alkanes of known isotopic values was daily injected into the system to check
227 the data quality and to ensure the analytical error to be ±0.5‰. Reported isotopic data

228 represent an averaged value of the multiple analyses.

229 3.4. Organic petrological examination

230 Crushed mudstone was prepared into polished blocks following the standard
231 preparation procedure described in Bustin et al. (1983). Observation of organic particles
232 was performed using a MPV-2 microscope.

233 4. Results

234 4.1. CaCO_3 and TOC concentrations

235 CaCO_3 concentrations in the Cretaceous samples range from 42.7% to 56.4%,
236 whereas those in the Paleocene range from 14.2% to 61.8% (Fig. 2). The concentration
237 drops to 25.4% at the top 0 horizon and stays low until LC-A-113.1. The concentration
238 increases to 53.3% at LC-A-129.7 and fluctuates between 22.6% and 61.8% for the rest
239 of the section (Fig. 2). TOC concentrations are extremely low (0.01% to 0.05%)
240 throughout the sequence and do not show any significant stratigraphic variation (Fig. 2).

241 4.2. Extractable organic compounds

242 Aliphatic hydrocarbon fractions are mainly composed of terrestrial higher
243 plant-derived long chain (C_{27} to C_{33}) *n*-alkanes. These *n*-alkanes are characterized by a
244 strong odd/even carbon number predominance (Fig. 3), as evidenced by high carbon
245 preference index (CPI_{29-33}) values of 3.7 to 6.0 for the upper Cretaceous samples and 1.8
246 to 7.4 for the Paleocene samples (Fig. 4). The concentrations of C_{29} and C_{31} *n*-alkanes
247 range from 0.4 to 39.0 ng/g dry sediment and 0.5 to 46.4 ng/g dry sediment,
248 respectively (Fig. 4). The C_{31} *n*-alkane is found as the most abundant homologue except
249 for samples LC-A-29.2 and LC-C-34.5 in which the C_{29} *n*-alkane dominates. The

250 occurrence of resin-derived higher plant biomarkers, i.e., aromatic terpenoids, is rare,
251 and higher plant-derived *n*-fatty acids and alcohols are not detected.

252 4.3. Stratigraphic fluctuations in the $\delta^{13}\text{C}$, ACL, and $\text{C}_{31}/(\text{C}_{29} + \text{C}_{31})$ values of *n*-alkanes

253 Fig. 4 shows the stratigraphic fluctuations of stable carbon isotopic
254 compositions ($\delta^{13}\text{C}$), average chain length (ACL₂₇₋₃₃) and $\text{C}_{31}/(\text{C}_{29} + \text{C}_{31})$ ratio of
255 *n*-alkanes. The $\delta^{13}\text{C}$ values of the C_{29} *n*-alkane range from -28.8‰ to -27.8‰ , whereas
256 those of the C_{31} *n*-alkanes range from -29.7‰ to -28.6‰ . The $\delta^{13}\text{C}$ values of the C_{31}
257 *n*-alkane are found to be more depleted in ^{13}C by up to 1.2‰ compared to the C_{29}
258 *n*-alkane throughout the section. The ACL and the $\text{C}_{31}/(\text{C}_{29} + \text{C}_{31})$ ratio range from 29.91
259 to 30.63 and 0.47 to 0.64, respectively. The ACL values are relatively low (29.91 to
260 30.17) in the lower Paleocene (LC-C-2 to LC-A-79.7), and the other proxies show
261 prominent negative excursions from LC-C-24.5 to LC-A-61.7 with peak values of 0.47
262 for the $\text{C}_{31}/(\text{C}_{29} + \text{C}_{31})$ ratio (LC-A-29.2) and of -28.8‰ (LC-C-40) and -29.5‰
263 (LC-C-40, 50) for the $\delta^{13}\text{C}$ of the C_{29} and C_{31} *n*-alkanes, respectively.

264 The stratigraphic profiles of the $\delta^{13}\text{C}$, ACL and $\text{C}_{31}/(\text{C}_{29} + \text{C}_{31})$ values enable
265 us to subdivide the section into four distinctive intervals (LC I–IV; Fig. 4). LC I is the
266 upper Cretaceous interval that is characterized by relatively constant values of the $\delta^{13}\text{C}$,
267 ACL and $\text{C}_{31}/(\text{C}_{29} + \text{C}_{31})$ ratio. LC II is the first 79.7 cm interval above the clastic
268 complex that is characterized by low ACL values and prominent negative shifts in the
269 $\text{C}_{31}/(\text{C}_{29} + \text{C}_{31})$ and $\delta^{13}\text{C}$ values. LC III is the interval between LC-A-79.7 and
270 LC-A-224.7 in which the $\delta^{13}\text{C}$ values and the ACL and $\text{C}_{31}/(\text{C}_{29} + \text{C}_{31})$ values vary in
271 opposite directions. LC IV covers the rest of the section, characterized by parallel trends
272 in these three parameters.

273 4.4. Microscopic observation of organic particles

274 Organic particles in two Paleocene samples (LC-C-2, LC-A-243.5) are mainly
275 composed of terrestrially derived tiny (<10 µm) vitrinite fragments. The occurrence of
276 these organic particles is rare, and the shapes of the fragments are subrounded to
277 subangular with medium to high reflectance. Organic particles derived from marine
278 organisms were not detected.

279 **5. Discussion**

280 *5.1. Transportation mechanism of terrestrial higher plant-derived n-alkanes*

281 Terrestrially derived organic matter is generally transported to marine
282 sediments by winds and fluvial processes (De Leeuw et al., 1995). The location of
283 Loma Capiro was more than 500 km south of its present position at the time of the
284 K–Pg event (Tada et al., 2003; Goto et al., 2008), and thus riverine delivery of organic
285 matter from the North American continent is unlikely due to the long transport distance
286 (>1,000 km; Fig. 1d). However, contributions from the nearby Cuban arc complex could
287 have occurred.

288 Because rivers can transport large quantities of particulate and dissolved
289 organic carbon from the continents (Hedges et al., 1997), sediments deposited near
290 rivers are expected to contain a significant amount of terrestrial organic matter.
291 However, the occurrence of higher plant derived particulate organic matter at Loma
292 Capiro is rare (See 4.4). In addition, low concentrations of resin-derived organic
293 compounds that are usually transported by rivers (Simoneit, 1977) such as retene
294 suggest that the riverine transport of terrigenous organic compounds had also been not
295 very significant at Loma Capiro.

296 According to model simulations of late Cretaceous atmospheric circulation,
297 the proto-Caribbean sedimentary basin was under the influence of the Northeast trade

298 winds (Cousin-Rittemard et al., 2002). Hence, the terrestrial higher plant-derived
299 *n*-alkanes at Loma Capiro are most likely to have been long-range transported via the
300 trade winds.

301 5.2. Stratigraphic fluctuations of the *n*-alkane $\delta^{13}\text{C}$ values across the K–Pg boundary

302 The $\delta^{13}\text{C}$ of terrestrial higher plants is primarily controlled by that in
303 atmospheric CO_2 (Farquhar et al., 1982; Arens et al., 2000). However, our $\delta^{13}\text{C}$ profiles
304 of terrestrial higher plant-derived *n*-alkanes exhibit only a weak negative shift ($\sim 0.3\text{‰}$)
305 in the lowermost Paleocene (LC II; Fig. 4), compared to the globally synchronous 1.5 to
306 2.0‰ negative excursion observed in the surface ocean-atmospheric carbon reservoir
307 (e.g. Hsü et al., 1982; Zachos and Arthur, 1986; Keller and Lindinger, 1989; Arinobu et
308 al., 1999; Arens and Jahren, 2000; 2002).

309 Similarly diminished excursions at the boundary have been reported in the
310 $\delta^{13}\text{C}$ values of bulk organic matter from Dogie Creek, Montana (Maruoka et al., 2007)
311 and Stevns Klint, Denmark (Brisman et al., 2001). These studies attributed such a small
312 shape of the excursions to an increased input of ^{13}C -enriched organic materials from
313 algae and wildfires. However, *n*-alkane contributions from these sources are not likely
314 to have occurred at Loma Capiro because relatively high CPI values of the *n*-alkanes
315 suggest that they originated exclusively from terrestrial higher plant waxes. In addition,
316 although the TOC concentrations of our samples are extremely low, a contamination
317 from contemporary plant sources is very unlikely because of the absence of long chain
318 *n*-fatty acids and alcohols, main constituents of contemporary plant leaf waxes as along
319 with the *n*-alkanes (Eglinton and Hamilton, 1967).

320 In general, there is a large input of ancient plant materials from soil to marine
321 sediments (Eglinton et al., 1997; Matsumoto et al., 2001). Thus, enhanced delivery of
322 these materials could have concealed the global ^{13}C -enriched signal. However, a marked

323 change in the *n*-alkane distributions before and after the K–Pg boundary (Fig. 3)
324 indicates a systematic change in their plant sources. Further, the averaged time lag in
325 delivery of soil organic matter (12,000 yrs; Eglinton et al., 1997; Matsumoto et al.,
326 2001) is too short to dilute the signal of the globally synchronous excursion spanning
327 more than several tens of thousands years (Arinobu et al., 1999; Arens and Jahren,
328 2000; Therrien et al., 2007).

329 Our lowermost Paleocene sample (LC-C-2) represents sediments that
330 deposited within the first 20,000 yrs following the K–Pg boundary (Alegret et al., 2005)
331 in which the $\delta^{13}\text{C}$ of terrestrial organic matter shows the globally synchronous excursion.
332 Thus, the $\delta^{13}\text{C}$ values of the *n*-alkanes at Loma Capiro should exhibit a 1.5 to 2.0‰
333 negative excursion in LC II if they reflected the global $\delta^{13}\text{C}$ signal. The absence of such
334 excursion suggests that our $\delta^{13}\text{C}$ records are likely affected by factors other than the
335 $\delta^{13}\text{C}$ variations in the exogenous carbon reservoir.

336 5.3. Factors controlling the *n*-alkane $\delta^{13}\text{C}$ values at Loma Capiro

337 The stable carbon isotopic compositions ($\delta^{13}\text{C}$) of terrestrial higher plants are
338 sensitive to photosynthetic carbon fixation pathways and isotopic fractionations that
339 reflect physiological responses to conditions in their growing environment, such as
340 continental aridity, light level, and growing temperature (Farquhar et al., 1982; Arens et
341 al., 2000), as well as taxonomic variations in contributing plant communities (Arens et
342 al., 2000; Chikaraishi and Naraoka, 2003). However, *n*-alkane contribution from C_4
343 plants is very unlikely at the time of the K–Pg boundary because the expansion of C_4
344 grass-dominated savannah did not occur until the Middle to Late Miocene (Jacobs et al.,
345 1999). Lower $\delta^{13}\text{C}$ values in C_{31} *n*-alkane as compared with C_{29} also suggest that the
346 *n*-alkanes unlikely originated from C_4 plants in which *n*-alkanes usually show nearly
347 constant isotopic composition across their different chain lengths (–17‰ to –24‰;

348 Collister et al., 1994; Kuypers et al., 1999).

349 In Fig. 5, we show a cross plot of the weighted-mean $\delta^{13}\text{C}$ values of the C_{29}
350 and C_{31} *n*-alkanes ($\delta^{13}\text{C}_{\text{WM}}$) and the $\text{C}_{31}/(\text{C}_{29} + \text{C}_{31})$ ratios from the four stratigraphic
351 intervals (LC I to IV). Although the correlations are not significant in LC I and LC IV,
352 the $\delta^{13}\text{C}_{\text{WM}}$ and the $\text{C}_{31}/(\text{C}_{29} + \text{C}_{31})$ values are positively correlated in LC II ($r = 0.89$; $p =$
353 0.04), whereas in LC III negatively correlated ($r = 0.91$; $p < 0.01$) (Fig. 5). Because the
354 chain length distribution of *n*-alkanes are sensitive to changes in the plant growing
355 environment and the composition of their source vegetation (Hall and Jones, 1961;
356 Poynter et al., 1989, Schefuß et al., 2003; Sachse et al., 2006), the presence of these
357 different trends in the $\delta^{13}\text{C}$ - $\text{C}_{31}/(\text{C}_{29} + \text{C}_{31})$ diagram suggests that the *n*-alkane $\delta^{13}\text{C}$
358 values are controlled by two types of paleoenvironmental factors in addition to the $\delta^{13}\text{C}$
359 of the exogenous carbon reservoir.

360 Contemporary observations reveal that important quantities of African dust
361 are carried across the equatorial Atlantic to the Caribbean via the trade winds (Prospero
362 and Lamb, 2003). Hence, the *n*-alkane signals at Loma Capiro likely represent
363 paleoenvironmental conditions of the northwestern part of the African continent
364 reflecting a wide zonal wind regime of the trade winds and a mixing during the
365 long-range transport.

366 *5.4. Environmental control on the n-alkane $\delta^{13}\text{C}$ values in the lower Paleocene (LC II)*

367 Several lines of evidence indicate enhanced greenhouse warming at the early
368 Paleocene as a result of the impact-induced CO_2 release from carbonate platforms and
369 the reduction of primary productivity (Hsü et al., 1982; O'Keefe and Ahrens, 1989).
370 Oxygen isotope records in marine carbonates reveal a period of gradual warming of
371 surface waters spanning a few hundred to several hundred thousand years following the
372 K–Pg boundary (Hsü et al., 1982; Zachos et al., 1989; Kaiho et al., 1999). At the same

373 time, records of plant leaf fossils and clay minerals also give evidence for increased
374 temperature and precipitation on land (Wolfe and Upchurch, 1987; Wolfe, 1990; Kaiho
375 et al., 1999), although a study on paleosols estimates a humid but cool climate in
376 western North America (Lehman, 1990). In the Southern Hemisphere, pollen
377 assemblages in New Zealand suggest transient warm humid conditions (Vajda et al.,
378 2001).

379 The stratigraphic variations of the $\delta^{13}\text{C}$ values show parallel decreases with
380 the ACL and $\text{C}_{31}/(\text{C}_{29} + \text{C}_{31})$ values in LC II (Fig. 4). In terms of plant physiology, such
381 decreases in these *n*-alkane proxies can be interpreted as plant responses to reduced
382 evapotranspiration. This response is because plants can alter the chain-length of leaf
383 waxes to minimize loss of water vapor from their leaves (Sachse et al., 2006). Under a
384 less evaporative condition, plants no longer need to reduce stomatal conductance to
385 conserve water in their leaves, which results in the $\delta^{13}\text{C}$ values becoming more ^{13}C
386 depleted (Farquhar et al., 1982). Hence, the concurrent decreases in the ACL and
387 $\text{C}_{31}/(\text{C}_{29} + \text{C}_{31})$ values and the $\delta^{13}\text{C}$ values in LC II seem to indicate a less evaporative
388 condition in the early Paleocene.

389 The age calculation based on the LSR for this interval indicates that the
390 duration of decreases in the $\delta^{13}\text{C}$, ACL and $\text{C}_{31}/(\text{C}_{29} + \text{C}_{31})$ values range from 9,700 to
391 37,000 yrs after the K-Pg boundary. This time period is consistent with that estimated
392 for the impact-induced warming (10^4 to 10^5 years; O'Keefe and Ahrens, 1989),
393 suggesting its relation to this transient warmth, although geochemical evidence indicates
394 that such warmth lasted only for a few thousand years following the boundary (Kaiho et
395 al., 1999). In contrast, the record of dinoflagellate cysts and benthic foraminifera at El
396 Kef, Tunisia, implies a ~2,000 yrs cooling following the K-Pg boundary in association
397 with an impact winter (Galeotti et al., 2004). Relatively high $\delta^{13}\text{C}$, ACL and $\text{C}_{31}/(\text{C}_{29} +$
398 $\text{C}_{31})$ values in our lowermost sample in the Paleocene (LC-C-2) might, thus, have been

399 resulted from plant responses to this cooling.

400 5.5. Vegetational control on the *n*-alkane $\delta^{13}\text{C}$ values in the lower Paleocene (LC III)

401 The $\text{C}_{31}/(\text{C}_{29} + \text{C}_{31})$ - $\delta^{13}\text{C}$ distributions exhibit marked differences between
402 before (LC I) and after (LC II) the K–Pg boundary, but the distribution of LC II
403 gradually shift back to the identical area as in the upper Cretaceous (LC I) through the
404 lower Paleocene (LC III; Fig. 5). Because the LC I and LC III distributions lie away
405 from the regression lines of LC II (Fig. 5), the shifts in the distributions should have
406 been controlled by some factor other than what caused the LC II variations (see 5.4).

407 In Fig. 6, we showed the stratigraphic profiles of the $\text{C}_{31}/(\text{C}_{29} + \text{C}_{31})$ ratio at
408 Loma Capiro and those in the K–Pg boundary sediments from Far East Asia (Mita and
409 Shimoyama, 1999). Interestingly, both $\text{C}_{31}/(\text{C}_{29} + \text{C}_{31})$ patterns exhibit similar decreases
410 following the K–Pg boundary. Such similarities between the sections that are >10,000
411 km apart indicate that the variations are likely resulted from a globally simultaneous
412 event, i.e., the K–Pg mass extinction.

413 At the K–Pg boundary, 15% to 57% of the late Cretaceous mega and
414 palynofloral species went extinct (e.g. Vajda and Raine, 2003; Wilf and Johnson, 2004;
415 Nichols, 2007). The devastated land flora was for a short period replaced by a fungal
416 community (Vajda and McLoughlin, 2004), which followed by the recovery succession
417 of photosynthetic plants that starts with a fern dominance, the so-called fern spike, in
418 North America, New Zealand and Far East Asia (Tschudy et al., 1984; Vajda et al.,
419 2001; Saito et al., 1986). In contrast, a rise of angiosperm and bryophyte floras are
420 reported in northern Canada and in the Netherlands, respectively (Sweet et al., 1990;
421 Brinkhuis and Schiøler, 1996). Vegetation with a diversity equivalent to that in the late
422 Cretaceous was subsequently established through angiosperm recolonization in North
423 America and tree ferns and gymnosperm dominances in New Zealand (Wolfe and

424 Upchurch, 1987; Vajda et al., 2001).

425 Although Méon (1990) concluded that no abrupt extinction occurred in
426 northwestern Africa, palynological data at El Kef, Tunisia, which is close to the possible
427 source area of leaf wax *n*-alkanes at Loma Capiro, show disappearance of 13.6% of the
428 upper Maastrichtian palynoflora at the boundary (Nichols and Johnson, 2008). Because
429 the C₃₁ *n*-alkane is generally more abundant in grasses and in certain species of other
430 angiosperms and conifers (Cranwell, 1973; Bi et al., 2005; Sachse et al., 2006;
431 Rommerskirchen et al., 2006), the good negative correlation between the *n*-alkane δ¹³C
432 values and the C₃₁/(C₂₉ + C₃₁) ratios in LC III might be attributed to vegetational
433 changes at the K–Pg boundary. In support for this idea, the C₃₁/(C₂₉ + C₃₁) variations
434 show good correspondence with an increase of the angiosperm/fern ratios in Far East
435 Asia (Fig. 6). However, there is no corresponding fern spore increase reported in
436 northwest Africa (Ben Abdelkader et al., 1997).

437 Based on the LSR of 2.0 cm/kyr for the lower Paleocene, the duration of LC
438 III is calculated as 40,000 to 67,000 yrs after the K–Pg boundary. This time period is
439 fairly longer than the time range for the fern dominance in Far East Asia and New
440 Zealand (several thousands of years; Vajda and Raine, 2003). Instead, it is rather close
441 to the duration taken for the recovery of the pre-boundary pollen assemblages in North
442 America (92,600 to 115,800 yrs; Therrien et al., 2007). Although the lack of a
443 palynological record at Loma Capiro does not allow us to assign any taxonomic
444 information, such correspondence in timing suggest that the δ¹³C and C₃₁/(C₂₉ + C₃₁)
445 variations in LC III are likely a consequence of the plant diversification process after
446 the K–Pg mass extinction.

447 **6. Conclusions**

448 The chain-length distribution [ACL and C₃₁/(C₂₉ + C₃₁) ratio] and stable

449 carbon isotopic compositions ($\delta^{13}\text{C}$) of sedimentary leaf wax *n*-alkanes were
450 investigated across the Cretaceous-Paleogene (K–Pg) boundary at Loma Capiro, Central
451 Cuba, to assess environmental and vegetational changes that are recorded in terrestrial
452 higher plants. The $\delta^{13}\text{C}$ profiles of the *n*-alkanes exhibit a negative excursion following
453 the K–Pg boundary. However, the magnitude of the excursion is much smaller ($\sim 0.3\text{‰}$)
454 than the global signals (1.5 to 2.0‰). The relations between the $\delta^{13}\text{C}$ and $\text{C}_{31}/(\text{C}_{29} + \text{C}_{31})$
455 ratios of the *n*-alkanes reveal that two types of paleoenvironmental factors (such as
456 temperature, humidity and vegetation) have affected this diminished $\delta^{13}\text{C}$ variation. The
457 *n*-alkanes at Loma Capiro are likely long-range transported by trade winds, and their
458 signals can be interpreted as reflecting paleoenvironmental conditions of the
459 northwestern part of the African continent. The *n*-alkane $\delta^{13}\text{C}$ values show a parallel
460 decrease with the ACL and $\text{C}_{31}/(\text{C}_{29} + \text{C}_{31})$ values in the first 37,000 yrs following the
461 K–Pg boundary, suggesting a possible influence of the impact-induced warm-humid
462 climate in the early Paleocene. In contrast, the *n*-alkane $\delta^{13}\text{C}$ values are negatively
463 correlated with the $\text{C}_{31}/(\text{C}_{29} + \text{C}_{31})$ ratios between 40,000 to 67,000 yrs after the K–Pg
464 boundary, suggesting that they likely reflect the plant diversification process after the
465 K–Pg mass extinction.

466 **Acknowledgements**

467 We thank the Japanese Society for Promotion of Science for financial support
468 through a Grant-in-Aid for Scientific Research (B) 17403005 (given to T. Matsui). We
469 also thank V. Vajda (Lund Univ., Sweden) and an anonymous reviewer for valuable
470 comments and suggestions. S.Y. expresses his deep appreciation to M. Ikehara (Kochi
471 Univ.) for assistance and organization of analyses at Kochi University and Y. Suzuki
472 (AIST) for kind assistance for the petrographic study of organic matter. M. Kato, T.
473 Kamiya, N. Hasebe, K. Moriya, T. Yamaguchi (Kanazawa Univ.), and E. Tajika (the

474 Univ. of Tokyo) provided constructive discussions and valuable suggestions, and P.A.
475 Meyers (The Univ. of Michigan) contributed with comments that improved the English.
476 This research was made possible thanks to an agreement between the Department of
477 Earth and Planetary Science, the University of Tokyo and the Museo Nacional de
478 Historia Natural (Agencia del Medio Ambiente) and the Instituto de Geología y
479 Paleontología del Ministerio de Industria Básica de Cuba. The research was also
480 performed under cooperative research program of the Center for Advanced Marine Core
481 Research (CMCR), Kochi University (06A008, 06B007 and 07A020).

482 **References**

- 483 Alegret, L., Arenillas, I., Arz, J. A., Díaz, C., Grajales-Nishimura, J. M., Meléndez, A.,
484 Molina, E., Rojas, R., Soria, A. R., 2005. Cretaceous–Paleogene boundary
485 deposits at Loma Capiro, central Cuba: evidence for the Chicxulub impact.
486 *Geology* 33, 721–724, doi: 10.1130/G21573.1.
- 487 Arenillas, I., Arz, J.A., Molina, E., 2004. A new high-resolution planktic foraminiferal
488 zonation and subzonation for the lower Danian. *Lethaia* 37, 79–95.
- 489 Arens, N. C., Jahren, A. H., 2000. Carbon isotope excursion in atmospheric CO₂ at the
490 Cretaceous–Tertiary boundary: evidence from terrestrial sediments. *Palaios* 15,
491 314–322.
- 492 Arens, N. C., Jahren, A. H., 2002. Chemostratigraphic correlation of four fossil-bearing
493 sections in southwestern North Dakota. In: Hartman, J. H., Johnson, K. R.,
494 Nichols, D. J. (Eds.), *The Hell Creek Formation and the Cretaceous–Tertiary*
495 *boundary in the northern Great Plains: an integrated continental record of the*
496 *end of the Cretaceous*, Geol. Soc. Amer. Boulder, CO, pp. 75–93.
- 497 Arens, N. C., Jahren, A. H., Amundson, R., 2000. Can C3 plants faithfully record the
498 carbon isotopic composition of atmospheric carbon dioxide? *Paleobiology* 26,

- 499 137–164.
- 500 Arinobu, T., Ishiwatari, R., Kaiho, K., Lamolda, M. A., 1999. Spike of pyrosynthetic
501 polycyclic aromatic hydrocarbons associated with an abrupt decrease in $\delta^{13}\text{C}$
502 of a terrestrial biomarker at the Cretaceous–Tertiary boundary at Caravaca,
503 Spain. *Geology* 27, 723–726.
- 504 Barrera, E., Keller, G., 1994. Productivity across the Cretaceous/Tertiary boundary in
505 high latitudes. *Bull. Geol. Soc. Amer.* 106, 1254–1266.
- 506 Ben Abdelkader, O., Ben Salem, H., Donze, P., Maamouri, A.-L., Méon, H., Robin, É.,
507 Rocchia, R., Froget, L., 1997. The K/T stratotype section of El Kef (Tunisia):
508 events and biotic turnovers. *GEOBIOS*, M.S.n° 21, 235–245.
- 509 Berggren, W.A., Kent, D.V., Aubry, M.-P., Hardenbol, J., 1995. Geochronology, time
510 scales and global stratigraphic correlation, *SEPM Spec. Pub.*, no. 54, 392p.
- 511 Bi, X., Sheng, G., Liu, X., Li, C., Fu, J., 2005. Molecular and carbon and hydrogen
512 isotopic composition of *n*-alkanes in plant leaf waxes. *Org. Geochem.* 36,
513 1405–1417.
- 514 Bralower, T.J., Paull, C.K., Leckie, R.M., 1998. The Cretaceous–Tertiary boundary
515 cocktail: Chicxulub impact triggers margin collapse and extensive sediment
516 gravity flows. *Geology* 26, 331–334.
- 517 Brinkhuis, H., Schiøler, P., 1996. Palynology of the Geulhemmerberg
518 Cretaceous/Tertiary boundary section (Limburg, SE Netherlands). *Geologie en*
519 *Mijnbouw* 75, 193–213.
- 520 Brisman, K., Engel, M. H., Macko, S. A., 2001. Distribution, stereochemistry, and
521 stable isotope composition of amino acids in K/T boundary sediments. *Precam.*
522 *Res.* 106, 59–77.
- 523 Bustin, R. M., Cameron, A. R., Grieve, D. A., Kalkreuth, W. D., 1983. Coal petrology,
524 its principles, methods, and applications. *Geol. Assoc. Can. Short Course Note*

- 525 3, Geol. Assoc. Can, Victoria.
- 526 Chikaraishi, Y., Naraoka, H., 2003. Compound-specific δD - $\delta^{13}\text{C}$ analyses of *n*-alkanes
527 extracted from terrestrial and aquatic plants. *Phytochemistry* 63, 361–371,
528 doi:10.1016/s0031-9422(02)00749-5.
- 529 Collister, J. W., Rieley, G., Stern, B., Eglinton, G., Fry, B., 1994. Compound-specific
530 $\delta^{13}\text{C}$ analyses of leaf lipids from plants with differing carbon dioxide
531 metabolisms. *Org. Geochem.* 21, 619–627.
- 532 Cousin-Rittemard, N. M. M., Dijkstra, H. A., Zwagers, T., 2002. Was there a
533 wind-driven Tethys circumglobal current in the Late Cretaceous? *Earth Planet.*
534 *Sci. Lett.* 203, 741–753.
- 535 Cranwell, P. A., 1973. Chain length distribution of *n*-alkanes from lake sediments in
536 relation to post-glacial environmental change. *Freshw. Biol.* 3, 259–265.
- 537 De Leeuw, J. W., Frewin, N. L., Van Bergen, P. F., Sinnighe Damsté, J. S., Coolinson, M.
538 E., 1995. Organic carbon as a palaeoenvironmental indicator in the marine
539 realm. In: Bosence, D. W. J., Allison, P. A. (Eds.), *Marine*
540 *Palaeoenvironmental Analysis from Fossils*, Geol. Soc., London, pp. 43–71.
- 541 D'Hondt, S., Zachos, J. C., 1993. On stable isotopic variation and earliest Paleocene
542 planktonic foraminifera. *Paleoceanography* 8, 527–547.
- 543 Eglinton, G., Hamilton, R. J., 1967. Leaf epicuticular waxes. *Science* 156, 1322–1335.
- 544 Eglinton, T. I., Benitez-Nelson, B. C., Pearson, A., McNichol, A. P., Bauer, J. E., Druffel,
545 E. R. M., 1997. Variability in radiocarbon ages of individual organic
546 compounds from marine sediments. *Science* 277, 796–799.
- 547 Farquhar, G. D., O'leary, M. H., Berry, J. A., 1982. On the relationship between carbon
548 isotope discrimination and the intercellular carbon dioxide concentration in
549 leaves. *Austral. Jour. Plant Physiol.* 9, 121–137.
- 550 Farquhar, G. D., Ehleringer, J. R., Hubick, K. T., 1989. Carbon isotope discrimination

551 and photosynthesis. *Annu. Rev. Plant Physiol. Plant Mol. Biol.* 40, 503–537.

552 Gagosian, R. G., Peltzer, E. T., 1986. The importance of atmospheric input of terrestrial
553 organic material to deep sea sediments. *Org. Geochem.* 10, 661–669.

554 Galeotti, S., Brinkhuis, H., Huber, M., 2004. Records of post-Cretaceous–Tertiary
555 boundary millennial-scale cooling from the western Tethys: A smoking gun for
556 the impact-winter hypothesis? *Geology* 32, 529–532.

557 Gilmour, I., Orth, C. J., Brooks, R. R., 1987. Carbon at a new K–T boundary site in
558 New Zealand. *Meteoritics* 22, 385–388.

559 Goto, K., Tada, R., Tajika, E., Iturralde-Vinent, M. A., Matsui, T., Yamamoto, S.,
560 Nakano, Y., Oji, T., Kiyokawa, S., García Delgado, D. E., Díaz Otero, C.,
561 Rojas Consuegra, R., 2008. Lateral lithological and compositional variations
562 of the Cretaceous/Tertiary deep-sea tsunami deposits in northwestern Cuba.
563 *Cret. Res.*, 29, 217–236.

564 Hall, D. M., Jones, R. L., 1961. Physiological significance of surface wax on leaves.
565 *Nature* 191, 95–96.

566 Hasegawa, T., Pratt, L. M., Maeda, H., Shigeta, Y., Okamoto, T., Kase, T. Uemura, K.,
567 2003. Upper Cretaceous stable carbon isotope stratigraphy of terrestrial
568 organic matter from Sakhalin, Russian Far East: proxy for the isotopic
569 composition of paleoatmospheric CO₂. *Palaeogeogr. Palaeoclimatol.*
570 *Palaeoecol.* 189, 97–115.

571 Hasegawa, T., Yamamoto, S., Pratt, L. M., 2006. Data report: stable carbon isotope
572 fluctuation of long-chain n-alkanes from Leg 208 Hole 1263A across the
573 Paleocene/Eocene boundary. In: Kroon, D., Zachos, J. C., Richter, C. (Eds.),
574 *Proc. ODP, Sci. Results 208*, College station, TX (Ocean Drilling Program), pp.
575 1–11. doi: 10.2973/odp.proc.sr.208.202.2006.

576 Hedges, J. I., Keil, R. G., Benner, R., 1997. What happens to terrestrial organic matter

577 in the ocean? *Org. Geochem.* 27, 195–212.

578 Hollander, D. J., McKenzie, J. A., Hsü, K. J., 1993. Carbon isotope evidence for
579 unusual plankton blooms and fluctuations of surface water CO₂ in
580 “Strangelove Ocean” after terminal Cretaceous event. *Palaeogeogr.*
581 *Palaeoclimatol. Palaeoecol.* 104, 229–237.

582 Hsü, K. J., He, Q., McKenzie, A., Weissert, H., Perch-Nielsen, K., Oberhänsli, H., Kelts,
583 K., LaBrecque, J., Tauxe, L., Krähenbühl, U., Percival, S. F. Jr., Wright, R.,
584 Karpoff, A. M., Petersen, N., Tucker, P., Poore, R. Z., Gombos, A. M.,
585 Pisciotto, K., Carman, M. F. Jr., Schreiber, E., 1982. Mass mortality and its
586 environmental and evolutionary consequences. *Science* 216, 249–256.

587 Jacobs, B. F., Kingston, J. D., Jacobs, L. L., 1999. The origin of grass-dominated
588 ecosystems. *Ann. Missouri Bot. Gard.* 86, 590–643.

589 Johnson, K. R., Nichols, D. J., Attrep Jr., M., Orth, C. J., 1989. High-resolution
590 leaf-fossil record spanning the Cretaceous/Tertiary boundary. *Nature* 340,
591 708–711.

592 Kaiho, K., Kajiwara, Y., Tazaki, K., Ueshima, M., Takeda, N., Kawahata, H., Arinobu,
593 T., Ishiwatari, R., Hirai, A., Lamolda, M. A., 1999. Oceanic primary
594 productivity and dissolved oxygen levels at the Cretaceous/Tertiary boundary:
595 their decrease, subsequent warming, and recovery. *Paleoceanography* 14,
596 511–524.

597 Keller, G., Lindinger, M., 1989. Stable isotope, TOC and CaCO₃ record across the
598 Cretaceous/Tertiary boundary at El Kef, Tunisia. *Palaeogeogr. Palaeoclimatol.*
599 *Palaeoecol.* 73, 243–265.

600 Kuypers, M. M. M., Pancost, R. D., Sinninghe Damsté, J. S., 1999. A large and abrupt
601 fall in atmospheric CO₂ concentration during Cretaceous times. *Nature* 399,
602 342–345.

- 603 Lehman, T. M., 1990. Paleosols and the Cretaceous/Tertiary transition in the Big Bend
604 region of Texas. *Geology* 18, 362–364.
- 605 Maruoka, T., Koeberl, C., Bohor, B. F., 2007. Carbon isotopic compositions of organic
606 matter across continental Cretaceous–Tertiary (K–T) boundary sections:
607 Implications for paleoenvironment after the K–T impact event. *Earth Planet.*
608 *Sci. Lett.* 253, 226–238.
- 609 Matsumoto, K., Kawamura, K., Uchida, M., Shibata, Y., Yoneda, M., 2001. Compound
610 specific radiocarbon and $\delta^{13}\text{C}$ measurements of fatty acids in a continental
611 aerosol sample. *Geophys. Res. Lett.* 28, 4587–4590.
- 612 Meyers, P. A., 1992. Changes in organic carbon isotope ratios across the K/T boundary:
613 global or local control? In: Macko, S. A., Engel, M. H. (Eds.), *Isotope*
614 *fractionations in organic matter: biosynthetic and diagenetic processes.* *Chem.*
615 *Geol. (Isot. Geosci. Sect.)* 101, 283–291.
- 616 Meyers, P. A., Simoneit, B. R. T., 1990. Global comparisons of organic matter in
617 sediments across the Cretaceous/Tertiary boundary. *Advances in Organic*
618 *Geochemistry 1989, Org. Geochem.* 16, 641–648.
- 619 Méon, H., 1990. Palynologic studies of the Cretaceous–Tertiary boundary interval at El
620 Kef outcrop, northwestern Tunisia: Paleogeographic implications. *Rev.*
621 *Palaeobot. Palynol.* 65, 85–94.
- 622 Mita, H., Shimoyama, A., 1999. Characterization of n-alkanes, pristane and phytane in
623 the Cretaceous/Tertiary boundary sediments at Kawaruppu, Hokkaido, Japan.
624 *Geochem. Jour.* 33, 285–294.
- 625 Nichols, D. J., 2007. Selected plant microfossil records of the terminal Cretaceous event
626 in terrestrial rocks, western North America. *Palaeogeogr. Palaeoclimatol.*
627 *Palaeoecol.* 255, 22–34, doi:10.1016/j.palaeo.2007.02.038.
- 628 Nichols, D.J., Johnson, K.R., 2008. *Plants and the K–T boundary.* Cambridge

- 629 University Press, New York.
- 630 Núñez-Cambra, K., Rojas-Consuegra, R., 2007. Elementos de la estructura de los
631 deslizamientos submarinos en los depósitos del límite K/T en Loma Capiro,
632 Santa Clara, Cuba central. Segunda Convención Cubana de Ciencias de La
633 Tierra, GEOCIENCIA' 2007. Centro Nacional de Información Geológica, IGP,
634 La Habana, pp. 103–104.
- 635 O'Keefe, J. D., Ahrens, T. J., 1989. Impact production of CO₂ by the
636 Cretaceous/Tertiary extinction bolide and the resultant heating of the Earth.
637 Nature 338, 247–249.
- 638 Orth, C. J., Gilmore, J. S., Knight, J. D., Pillmore, C. L., Tshudy, R. H., Fassett, J. E.,
639 1981. An iridium anomaly at the palynological Cretaceous–Tertiary boundary
640 in northern New Mexico. Science 214, 1341–1343.
- 641 Pancost, R. D., Boot, C. S., 2004. The palaeoclimatic utility of terrestrial biomarkers in
642 marine sediments. Mar. Chem. 92, 239–261.
- 643 Poynter, J. G., Farrimond, P., Robinson, N., Eglinton, G., 1989. Aeolian-derived higher
644 plant lipids in the marine sedimentary record: links with palaeoclimate. In:
645 Leinen, M., Sarnthein, M. (Eds.), Paleoclimatology and paleometeorology:
646 modern and past patterns of global atmospheric transport, Kluwer Academic
647 Publishers, Dordrecht, The Netherlands, pp. 435–462.
- 648 Prospero, J. M., Lamb, P. J., 2003. African droughts and dust transport to the Caribbean:
649 climate change implications. Science 302, 1024–1027,
650 doi:10.1126/science.1089915.
- 651 Raup, D. M., Sepkoski, J. J. Jr., 1982. Mass extinctions in the marine fossil record.
652 Science 215, 1501–1503.
- 653 Rojas-Consuegra, R., Iturralde-Vinent, M. A., Díaz-Otero, C., García-Delgado, D.,
654 Meléndez-Evia, A., Soria, A. R., 2005. Significación paleogeográfica de la

655 brecha basal del Límite K/T en Loma Dos Hermanas (Loma Capiro) en Santa
656 Clara, provincia de Villa Clara. Primera Convención Cubana de Ciencias de la
657 Tierra. Geociencias 8, 1–9.

658 Rojas-Consuegra, R., Díaz-Otero, C., Meléndez, A., Soria, A. R., 2007. Depósito del
659 Límite K–T en Loma Capiro: nueva formación geológica en Cuba central.
660 Segunda Convención Cubana de Ciencias de La Tierra, GEOCIENCIA' 2007.
661 Centro Nacional de Información Geológica, IGP, La Habana, pp. 104–105.

662 Rommerskirchen, F., Eglinton, G., Dupont, L., Günter, U., Wenzel, C., Rullkötter, J.,
663 2003. A north to south transect of Holocene southeast Atlantic continental
664 margin sediments: Relationship between aerosol transport and
665 compound-specific $\delta^{13}\text{C}$ land plant biomarker and pollen records. *Geochem.*
666 *Geophys. Geosyst.* 4(12), 1101, doi:10.1029/2003GC000541.

667 Rommerskirchen, F., Plader, A., Eglinton, G., Chikaraishi, Y., Rullkötter, J., 2006.
668 Chemotaxonomic significance of distribution and stable carbon isotopic
669 composition of long-chain alkanes and alkan-1-ols in C_4 grass waxes. *Org.*
670 *Geochem.* 37, 1303–1332.

671 Sachse, D., Radke, J., Gleixner, D., 2006. δD values of individual *n*-alkanes from
672 terrestrial plants along a climatic gradient – implications for the sedimentary
673 biomarker record. *Org. Geochem.* 37, 469–483.

674 Saito, T., Yamanoi, T., Kaiho, K., 1986. End-Cretaceous devastation of terrestrial flora
675 in the boreal Far East. *Nature* 323, 253–255.

676 Schefuß, E., Ratmeyer, V., Stuut, J.-B. W., Jansen, J. H. F., Sinninghe Damsté, J. S.,
677 2003. Carbon isotope analysis of *n*-alkanes in dust from the lower atmosphere
678 over the central eastern Atlantic. *Geochim. Cosmochim. Acta* 67, 1757–1767.

679 Schimmelmann, A., Deniro, M. J., 1984. Elemental and stable isotope variations of
680 organic matter from a terrestrial sequence containing the Cretaceous/Tertiary

681 boundary at York Canyon, New Mexico. *Earth Planet. Sci. Lett.* 68, 392–398.

682 Schulte, P., Speijer, R., Mai, H., Kontny, A., 2006. The Cretaceous–Paleogene (K–P)

683 boundary at Brazos, Texas: sequence stratigraphy, depositional events and the

684 Chicxulub impact. *Sediment. Geol.* 184, 77–109.

685 Schulte, P., Alegret, L., Arenillas, I., Arz, J.A., Barton, P.J., Bown, P.R., Bralower, T.J.,

686 Christeson, G.L., Claeys, P., Cockell, C.S., Collins, G.S., Deutsch, A., Goldin,

687 T.J., Goto, K., Grajales-Nishimura, J.-M., Grieve, R.A.F., Gulick, S.P.S.,

688 Johnson, K.R., Kiessling, W., Koeberl, C., Kring, D.A., MacLeod, K.G.,

689 Matsui, T., Melosh, J., Montanari, A., Morgan, J.V., Neal, C.R., Nichols, D.J.,

690 Norris, R.D., Pierazzo, E., Ravizza, G., Rebolledo-Vieyra, M., Reimold, W.U.,

691 Robin, E., Salge, T., Speijer, R.P., Sweet, A.R., Urrutia-Fucugauchi, J., Vajda,

692 V., Whalen, M.T., Willumsen, P.S., 2010. The Chicxulub Asteroid Impact and

693 Mass Extinction at the Cretaceous–Paleogene Boundary. *Science* 327,

694 1214–1218.

695 Simoneit, B.R.T., 1977. Diterpenoid compounds and other lipids in deep-sea sediments

696 and their geochemical significance. *Geochim. Cosmochim. Acta* 41, 463–476.

697 Smit, J., 1982. Extinction and evolution of planktonic foraminifera after a major impact

698 at the Cretaceous/Tertiary boundary. *Geol. Soc. Am. Spec. Pap.* 190, 329–352.

699 Smit, J., Roep, T.B., Alvarez, W., Montanari, A., Claeys, P., Grajales-Nishimura, J.M.,

700 Bermudez, J., 1996. Coarse-grained, clastic sandstone complex at the K/T

701 boundary around the Gulf of Mexico: Deposition by tsunami waves induced

702 by the Chicxulub impact? In: Ryder, G., Fastovsky, D., Gartner, S. (Eds.), *The*

703 *Cretaceous–Tertiary event and other catastrophes in Earth history.* *Geol. Soc.*

704 *America, Boulder, CO*, pp. 151–182

705 Sweet, R., Braman, D. R., Lerbekmo, J. F., 1990. Palynofloral response to K/T

706 boundary events: a transitory interruption within a dynamic system.

707 In: Sharpton, V. L., Ward, P. D. (Eds.), *Global Catastrophes in Earth History:*
708 *an Interdisciplinary Conference on Impacts, Volcanism, and Mass*
709 *Mortality.* Geol. Soc. America, Boulder, CO, pp. 457–469.

710 Tada, R., Iturralde-Vinent, M. A., Matsui, T., Tajika, E., Oji, T., Goto, K., Nakano, Y.,
711 Takayama, H., Yamamoto, S., Kiyokawa, S., Toyoda, K., García-Delgado, D.,
712 Díaz-Otero, C., Rojas-Consuegra, R., 2003. K/T boundary deposits in the
713 paleo-western Caribbean basin. In: Bartolini, C., Buffler, R. T., Blickwede, J.
714 (Eds.), *The Circum-Gulf of Mexico and the Caribbean: Hydrocarbon habitats,*
715 *basin formation, and plate tectonics,* AAPG Memoir 79, pp. 582–604.

716 Therrien, F., Eberth, D. A., Braman, D. R., Zelenitsky, D. K., 2007. High-resolution
717 organic carbon isotope record across the Cretaceous–Tertiary boundary in
718 south-central Alberta: implications for the post-impact recovery rate of
719 terrestrial ecosystems and use of $\delta^{13}\text{C}$ as a boundary marker. *Can. Jour. Earth*
720 *Sci.* 44, 529–542.

721 Tschudy, R. H., Pillmore, C. L., Orth, C. J., Gilmore, J. S., Knight, J. D., 1984.
722 Disruption of the terrestrial plant ecosystem at the Cretaceous–Tertiary
723 boundary, Western Interior. *Science* 225, 1030–1032.

724 Vajda, V., Raine, J. I., 2003. Pollen and spores in marine Cretaceous/Tertiary boundary
725 sediments at mid-Waipara River, North Canterbury, New Zealand. *New*
726 *Zealand Jour. Geol. Geophys.* 46, 255–273.

727 Vajda, V., MacLoughlin, S., 2004. Fungal proliferation at the Cretaceous–Tertiary
728 Boundary. *Science* 303, 1489.

729 Vajda, V., Raine, J. I., Hollis, C. J., 2001. Indication of global deforestation at the
730 Cretaceous–Tertiary boundary by New Zealand fern spike. *Science* 294,
731 1700–1702.

732 Wilf, P., Johnson, K. R., 2004. Land plant extinction at the end of the Cretaceous: a

- 733 quantitative analysis of the North Dakota megafloral record. *Paleobiology* 30,
734 347–368.
- 735 Wolfe, J. A., 1990. Palaeobotanical evidence for a marked temperature increase
736 following the Cretaceous/Tertiary boundary. *Nature* 343, 153–156.
- 737 Wolfe, J. A., Upchurch, G. R. Jr., 1987. Leaf assemblages across the
738 Cretaceous–Tertiary boundary in the Raton Basin, New Mexico and Colorado.
739 *Proc. Natl. Acad. Sci. USA* 84, 5096–5100.
- 740 Zachos, J. C., Arthur, M. A., 1986. Paleooceanography of the Cretaceous/Tertiary
741 boundary event: inferences from stable isotopic and other data.
742 *Paleoceanography* 1, 5–26.
- 743 Zachos, J. C., Arthur, M. A., Dean, W. E., 1989. Geochemical evidence for suppression
744 of pelagic marine productivity at the Cretaceous/Tertiary boundary. *Nature* 337,
745 61–64.

746 **Figure captions**

747 **Fig. 1.** Map showing the location of (a) Santa Clara, (b) Loma Capiro, (c) distribution
748 of the exposure at Loma Capiro, (d) paleogeotectonic setting of Loma Capiro at the
749 Cretaceous–Paleogene boundary (modified after Goto et al., 2008).

750 **Fig. 2.** Stratigraphy, lithology, samples and bulk geochemistry (calcium carbonate and
751 total organic carbon content) of the Cretaceous–Paleogene section at Loma Capiro.
752 *adapted from Alegret et al. (2005). Abbreviation: Cret.; Cretaceous, *A. maya.*;
753 *Abathomphalus mayaroensis* Zone. Note the change in scale due to the presence of a
754 clastic complex at the base of the Paleogene.

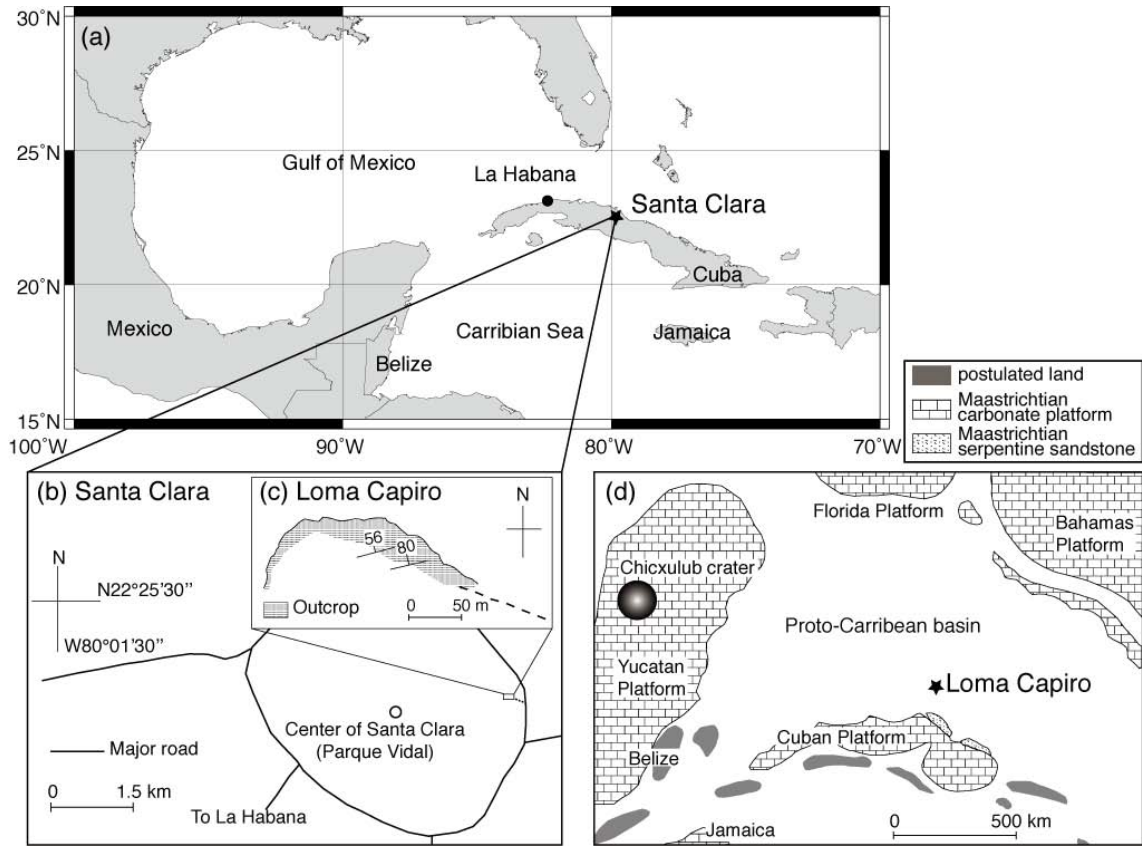
755 **Fig. 3.** Gas chromatograms of aliphatic hydrocarbon fraction obtained from (a)
756 Cretaceous and (b) Paleogene samples. Numbers on the GC peaks indicate the
757 carbon chain length of *n*-alkanes. The carbon preference index (CPI) values are also
758 displayed.

759 **Fig. 4.** Stratigraphic profiles of (a) concentration, (b) carbon preference index (CPI), (c)
760 stable carbon isotope ratios ($\delta^{13}\text{C}$), (d) $\text{C}_{31}/(\text{C}_{29} + \text{C}_{31})$ ratio and (e) average chain
761 length (ACL) of leaf wax *n*-alkanes in the sediments, which can be separated into
762 four distinctive intervals (LC I to LC IV). For legend and abbreviations, refer Fig. 2.

763 **Fig. 5.** Cross-plot of the weighted-mean $\delta^{13}\text{C}$ of C_{29} and C_{31} *n*-alkanes ($\delta^{13}\text{C}_{\text{WM}}$) versus
764 $n\text{-C}_{31}/(n\text{-C}_{29} + n\text{-C}_{31})$ ratio. Although relations are not significant in LC I and IV, the
765 $\delta^{13}\text{C}_{\text{WM}}$ and $\text{C}_{31}/(\text{C}_{29} + \text{C}_{31})$ values are positively correlated in LC II ($r = 0.89$; $p =$
766 0.04), and are negatively correlated in LC III ($r = 0.91$; $p < 0.01$).

767 **Fig. 6.** Comparison of the stratigraphic variations of (a) $\text{C}_{31}/(\text{C}_{29} + \text{C}_{31})$ ratio at Loma
768 Capiro, and (b) $\text{C}_{31}/(\text{C}_{29} + \text{C}_{31})$ ratio and (c) floral composition in Far East Asia
769 across the Cretaceous–Paleogene boundary. *Berggren et al. (1995); **Smit
770 (1982); ***Arenillas et al. (2004).

771



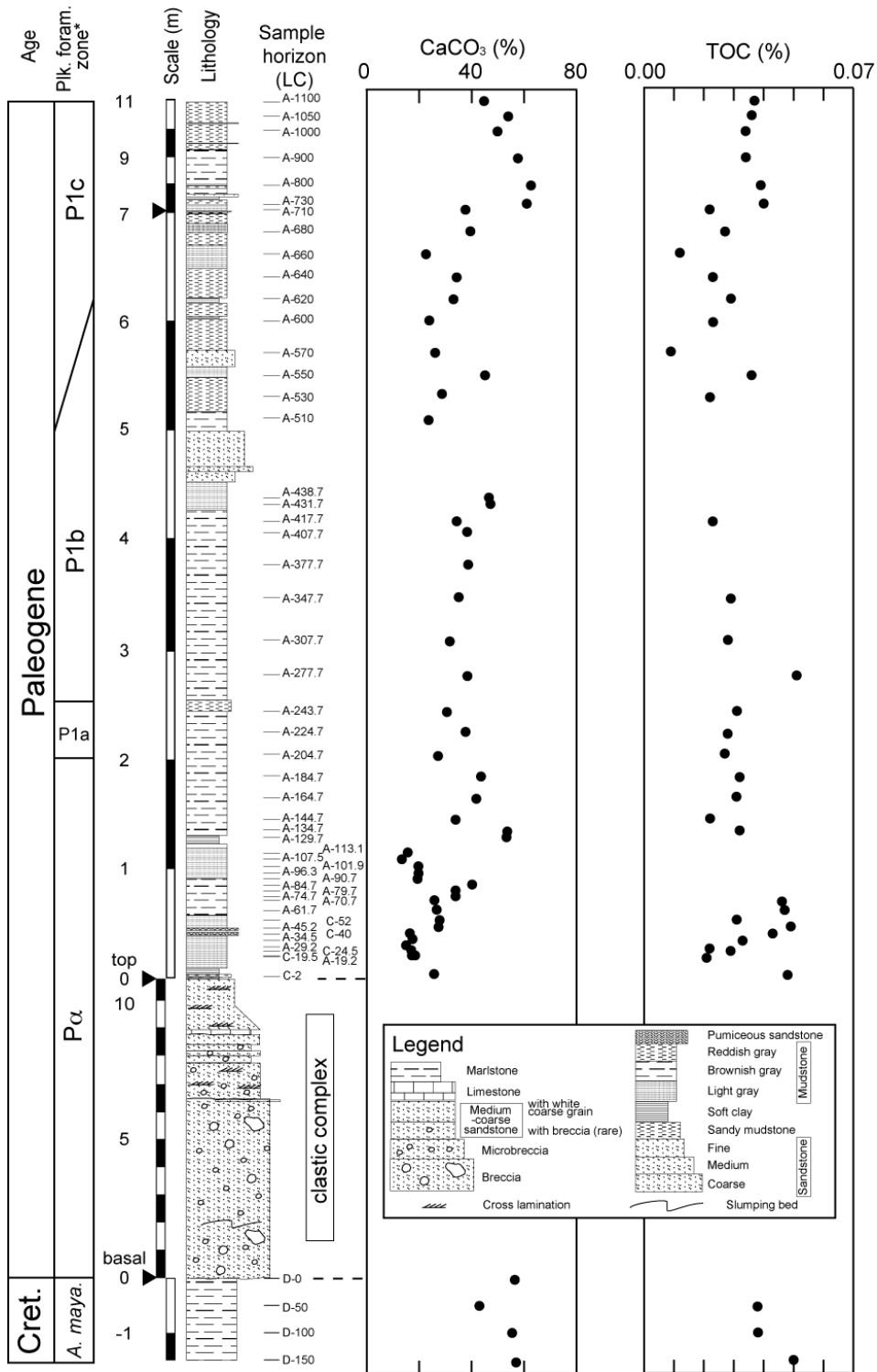
771

772

773

774

Fig. 1



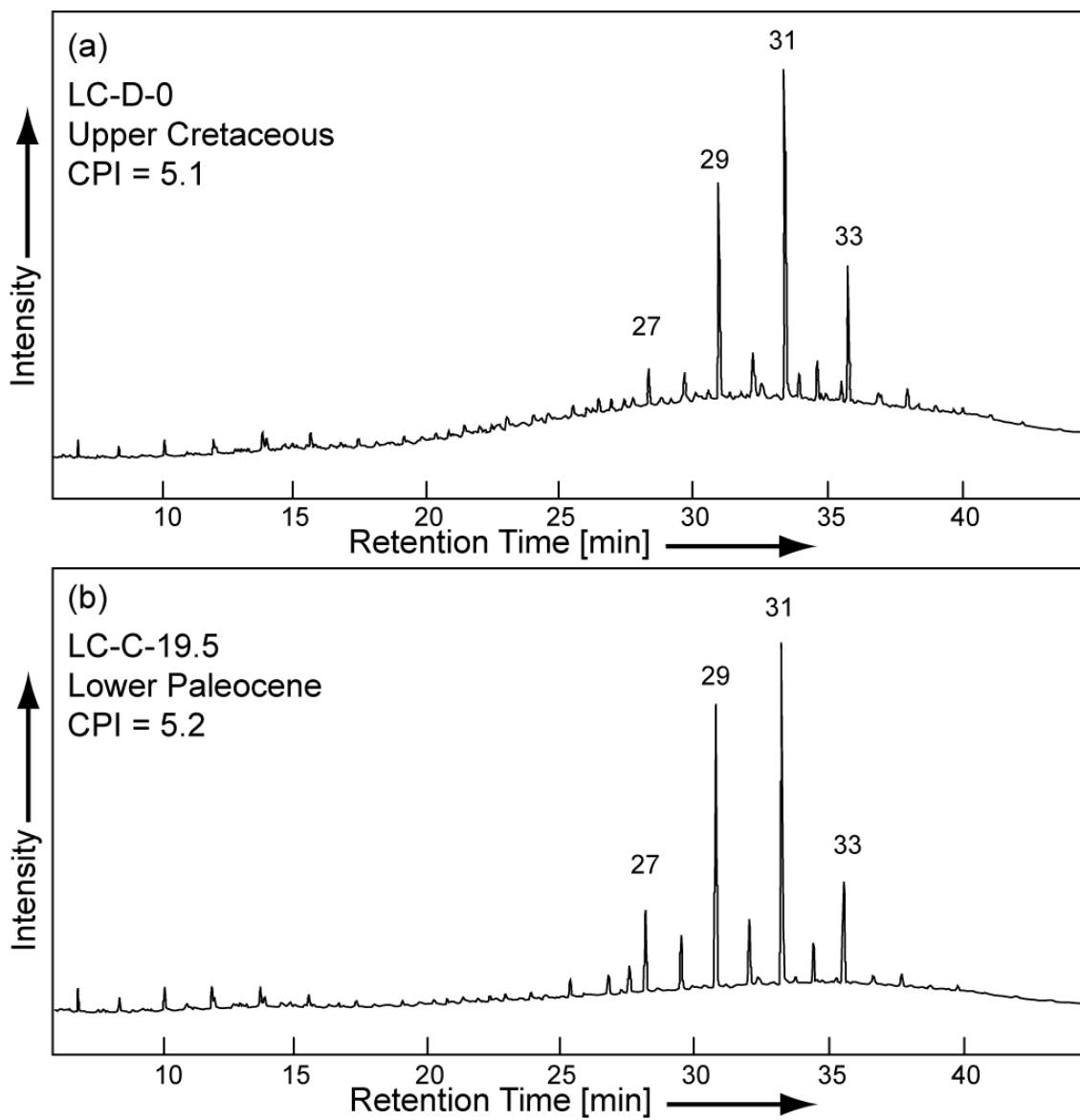
774

775

776

777

Fig. 2



777

778

779

780

Fig. 3

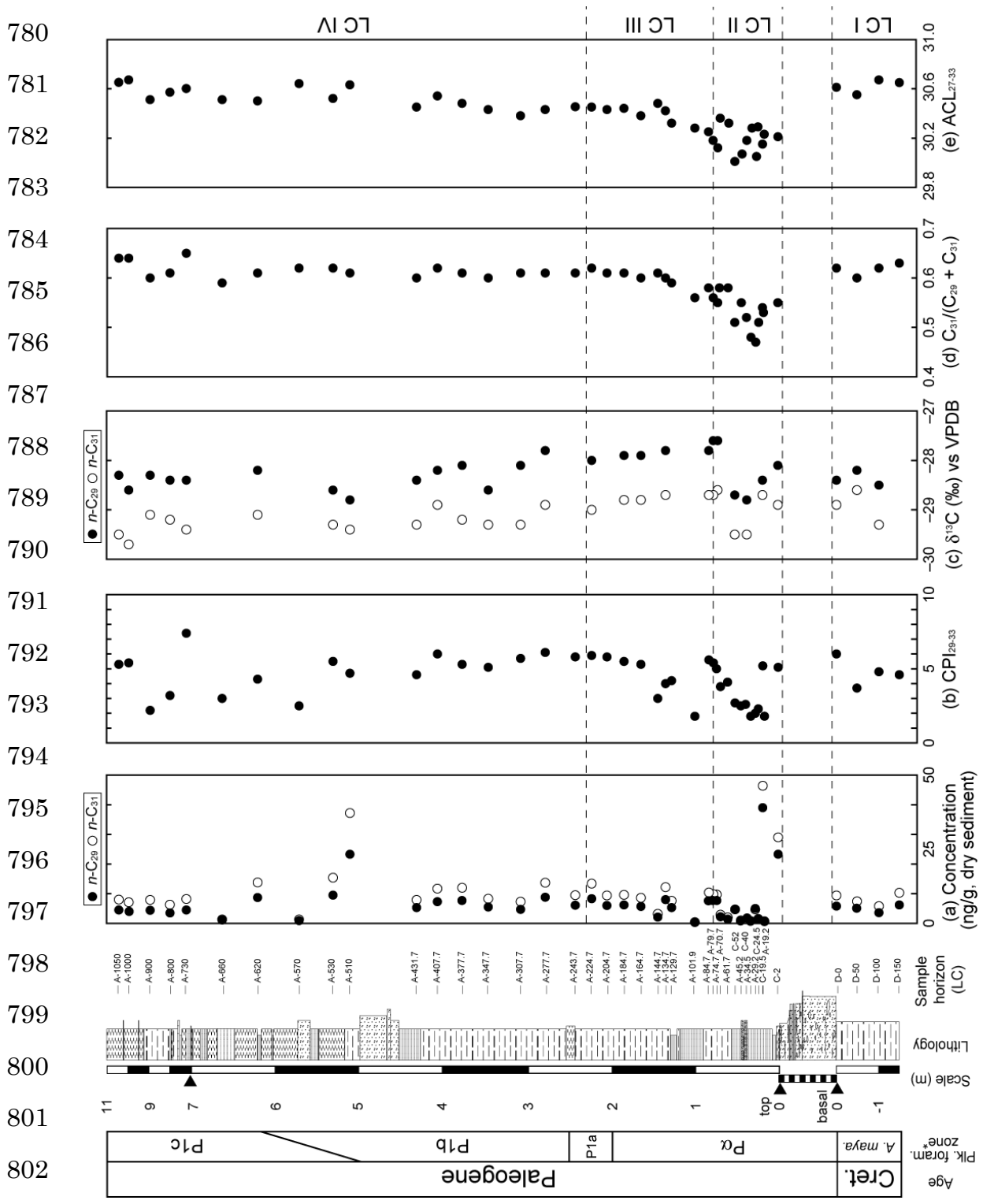
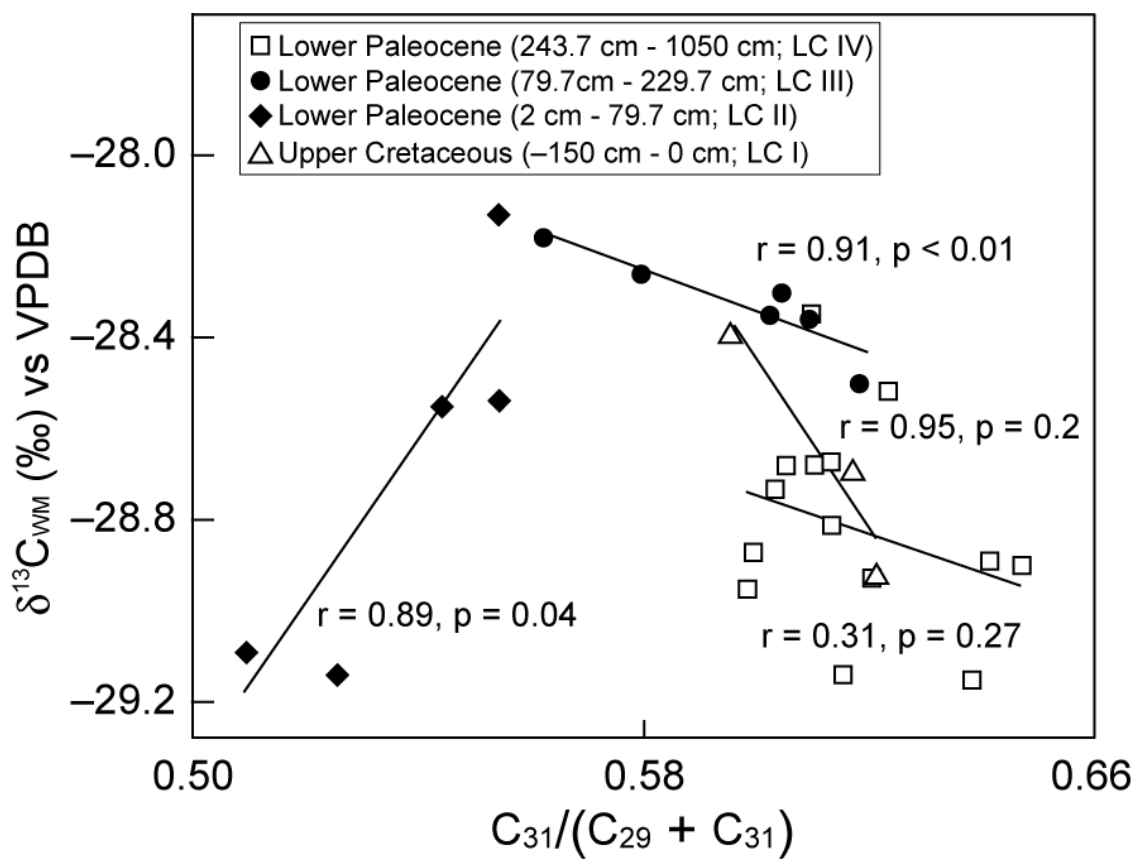


Fig. 4



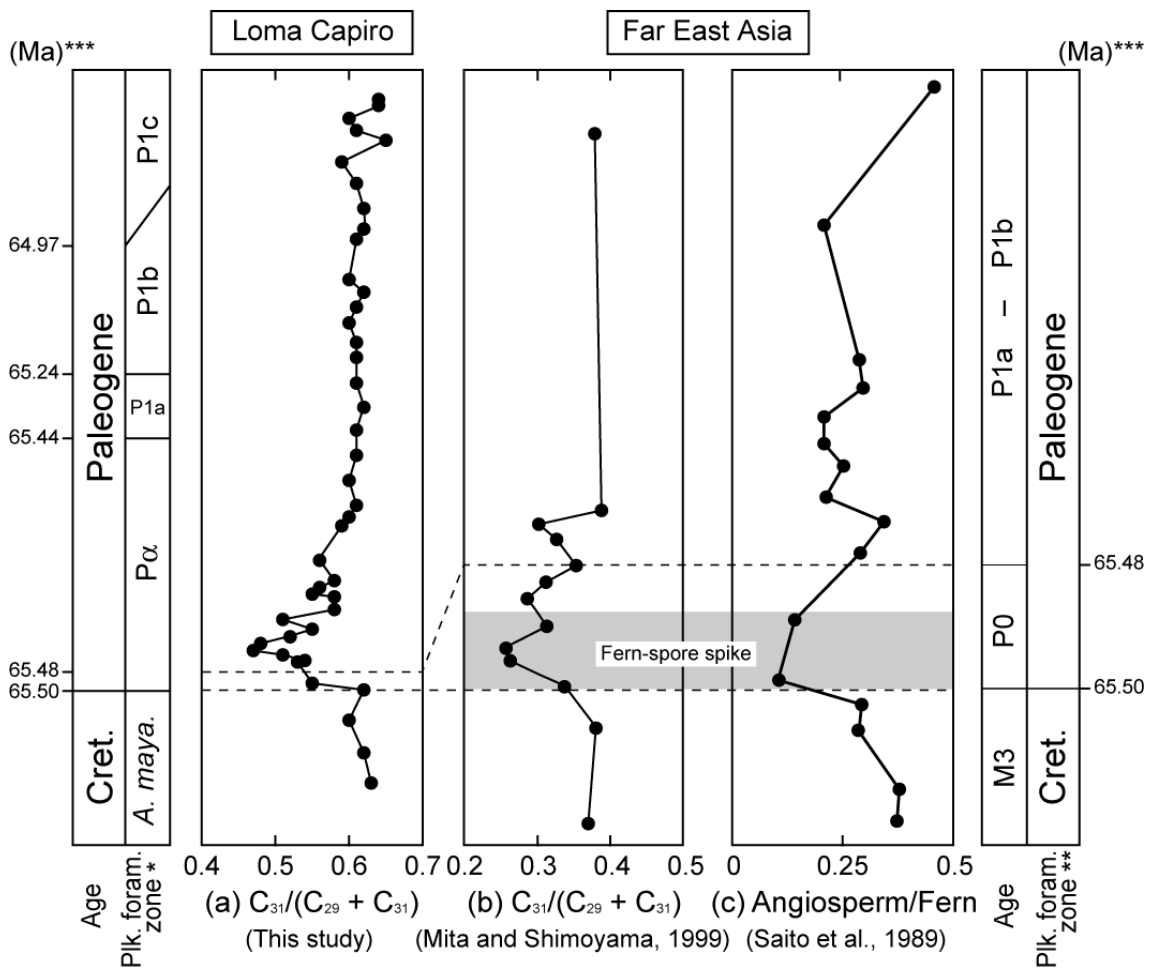
806

807

808

809

Fig. 5



809

810

811

Fig. 6